Detection of synchronization between chaotic signals: An adaptive similarity-based approach

Shyan-Shiou Chen,[1,*] Li-Fen Chen,[2,3] Yu-Te Wu,[2,3,4] Yu-Zu Wu,[5] Po-Lei Lee,[2,3,6] Tzu-Chen Yeh,[2,3,7] and Jen-Chuen Hsieh[2,3,7,8,9,†]

[1]*Department of Mathematics, National Taiwan Normal University, Taipei, Taiwan*
[2]*Institute of Brain Science, National Yang-Ming University, Taipei, Taiwan*
[3]*Integrated Brain Research Laboratory, Department of Medical Research and Education, Taipei Veterans General Hospital, Taipei, Taiwan*
[4]*Department of Biomedical Imaging and Radiological Sciences, National Yang-Ming University, Taipei, Taiwan*
[5]*Department of Physical Therapy, Tzu-Chi College of Technology, Hualien, Taiwan*
[6]*Department of Electrical Engineering, National Central University, Taiwan*
[7]*Faculty of Medicine, School of Medicine, National Yang-Ming University, Taipei, Taiwan*
[8]*Institute of Neuroscience, School of Life Science, National Yang-Ming University, Taipei, Taiwan*
[9]*Brain Research Center, National Yang-Ming University, Taiwan*

(Received 21 May 2007; revised manuscript received 29 August 2007; published 19 December 2007)

We present an adaptive similarity-based approach to detect generalized synchronization (GS) with $n:m$ phase synchronization (PS), where n and m are integers and one of them is 1. This approach is based on the similarity index (SI) and Gaussian mixture model with the minimum description length criterion. The clustering method, which is shown to be superior to the closeness and connectivity of a continuous function, is employed in this study to detect the existence of GS with $n:m$ PS. We conducted a computer simulation and a finger-lifting experiment to illustrate the effectiveness of the proposed method. In the simulation of a Rössler-Lorenz system, our method outperformed the conventional SI, and GS with 2:1 PS within the coupled system was found. In the experiment of self-paced finger-lifting movement, cortico-muscular GS with 1:2 and 1:3 PS was found between the surface electromyogram signals on the first dorsal interossei muscle and the magnetoencephalographic data in the motor area. The GS with $n:m$ PS (n or $m=1$) has been simultaneously resolved from both simulation and experiment. The proposed approach thereby provides a promising means for advancing research into both nonlinear dynamics and brain science.

DOI: 10.1103/PhysRevE.76.066208 PACS number(s): 05.45.−a, 05.90.+m, 87.90.+y, 89.75.Fb

I. INTRODUCTION

The core problems of synchronization in brain science are how to sensitively detect the interdependence among dynamical variables within each coupled chaotic biological system and what kinds of functional connectivity are across specialized brain regions. Conventional linear methods based on the cross-correlation and coherence function are limited to the detection of linear features of biological signals, and, thereby, many works have been instigated to develop tools for resolving the nonlinear interdependence. In the literature, two types of nonlinear interdependence, including phase synchronization (PS) and generalized synchronization (GS), have been recognized as key nonlinear features of functional connectivity in brain science [1–12]. It was proposed that GS always leads to PS, but not vice versa. To our knowledge, the coexistence of GS and $1:m$ PS ($m>1$) for data analysis has been less explored in the literature, even though these two types of synchronization had been, respectively, discussed in different fields. It is of potential importance to develop a general method to detect the coexistence of these two types of synchronization in a coupled system, especially in biological systems.

The PS in a coupled chaotic system means that the phases between systems are locked whether their amplitudes are correlated or not. That is, the phases of one system can be predicted by the phases of the other. Many methods have been developed to extract the phases of univariate and multivariate time series. In the case of a univariate time series associated with a principal frequency, one can decompose the time series into instantaneous phase and amplitude sequences by means of convolution with a Gabor wavelet centered at a frequency or Hilbert transformation. Based on these two respective transformations, $n:m$ PS could be detected by the methods of phase-locking statistics [11] and Shannon entropy [12], correspondingly. In 2001, Le Van Quyen *et al.* [13] further concluded that the results obtained from these two methods are fundamentally equivalent for the study of neuroelectrical signals. In the case of a multivariate time series with clear rotations on the phase portrait projection—e.g., Rössler system—a phase increase of 2π can be associated with a successive crossing with an appropriate secant surface. The phases in between can therefore be computed with a linear interpolation [14]. For these methods of phase extraction, the former determines phases in the temporal domain, the latter in the spatial domain. By the transformation of a time-delayed phase reconstruction [15], the univariate time series can be transformed to a multivariate one. Takens [15] and Saur *et al.* [16] theoretically proved that there exists a diffeomorphism between its underlying

*sschen@ntnu.edu.tw
†Corresponding author. Brain Research Center and Institute of Brain Science, National Yang-Ming University, No. 155, Sec. 2, Linong St. Taipei 112 Taiwan. jchsieh@ym.edu.tw Tel: +886–2–28267906 Fax: +886–2–28745182

true trajectories and its time-delayed reconstructed multivariate one. The phases in the reconstructed multivariate case can be possibly equivalent to those in the univariate one. It should be noted that the PS in most experiments was detected not in the spatial domain, but in the temporal domain. The development of a general method for detecting PS in the spatial domain should be further investigated.

In a coupled chaotic system, the dynamics will collapse onto an attractor of the full phase space when GS occurs [17]. It implies the existence of a certain functional relationship between these subsystems. Under the circumstance of a continuous function between the attractors of two subsystems, the contemporary points in the other subsystem will be close to each other when the points in the phase space of one subsystem approximate each other. In general, two time series with a functional relationship do not necessarily connote resemblance between each other. Previous studies [18–20] used the average translation of mutual neighbors as a predictor of the driver system to describe the interaction between a driver-response system. Arnhold *et al.* [21] proposed the similarity index (SI) to investigate the nonlinear interdependence for the intracranially recorded electroencephalograms of epileptic patients. Stam *et al.* [1] proposed the synchronization likelihood, which could exclude the bias pointed out by Pereda *et al.* [22], for early Alzheimer disease to infer the clinical mechanisms. These three studies were based on the existence of the closeness and connectivity in a spatial domain. It is worthy to note that the closeness and connectivity are necessary for the continuous function in a Euclidean space and are candidates to reveal the underlying relationship between the two time series. However, the mapping between two chaotic attractors is in general unknown, which makes the closeness and connectivity difficult to be satisfied.

The present study utilizes the clustering technique to detect GS with $1:m$ PS ($m>1$), which was not mentioned in [21,23,24]. Specifically, the mapping between two chaotic attractors is characterized by clusters, instead of the closeness and connectivity of a continuous function. Notably, in this case, the clustering nature in a spatial domain in place of the conventional phase difference in a temporal domain was dynamically detected by the Gaussain mixture model with the minimum description length (MDL) criterion. This is different from the classical methods mentioned in the previous paragraphs. This paper is organized as follows. Section II introduces the adaptive similarity-based index and Gaussian mixture model with the MDL criterion. Section III analyzes the simulation data from a Rössler-Lorenz system and the physiological signals from 2-Hz cued self-paced finger movements. Section IV discusses the clustering characteristic in the spatial domain. Section V concludes this study.

II. ADAPTIVE SIMILARITY-BASED APPROACH

Let x_n be a scalar time series. By the time-delay procedure [15,16], we can construct a d_x-dimensional vector $\mathbf{x}_n$ with coordinates $(x_n,\ldots,x_{n+(d_x-1)\tau})$. Herein, the delay time τ_x is chosen by the first minimum of mutual information [25] and the embedding dimension d_x is determined by computing the ratio of false nearest neighbors [26]. A reconstructed trajectory $\mathbf{X}$ denotes the collection of the points, $\mathbf{x}_1^{\mathrm{T}},\mathbf{x}_2^{\mathrm{T}},\ldots$, where T denotes transpose. For different time series, we can compute the values of the corresponding items and define their symbols by the same process.

Let Γ_n^k (Ω_n^k) denote the collection of time indices of the k nearest neighbors (KNN) of $\mathbf{x}_n$ ($\mathbf{y}_n$), where $\Gamma_n^k=\{\gamma_{n,j}|j=1,\ldots,k\}$ ($\Omega_n^k=\{\omega_{n,j}|j=1,\ldots,k\}$). The KNN of $\mathbf{x}_n$ are called *actual neighbors*. Let $\mathbf{x}(\Omega_n^k)$ denote the set of points by $\{\mathbf{x}_{\omega_{n,j}}|j=1,\ldots,k\}$ and be called *mutual neighbors*. Correspondingly, the sets $\mathbf{y}(\Omega_n^k)$ and $\mathbf{y}(\Gamma_n^k)$ are actual neighbors and mutual neighbors, respectively. The index of the actual (mutual) neighbors is called the *driver* (*response*) *index*. For every $\mathbf{x}_n\in\mathbb{R}^{d_x}$, we define the mean Euclidean distance for the set of $\mathbf{x}_n$ and its actual neighbors as $V_n^{(k)}(\mathbf{X})=\frac{1}{k}\Sigma_{i=1}^k\|\mathbf{x}_{\gamma_n}-\mathbf{x}_{\gamma_{n,i}}\|^2$. Assume that the mutual neighbors $\mathbf{x}(\Omega_n^k)$ can be modeled by the Gaussian mixture model (GMM) as follows:

$$p(\xi|\Theta,\mathbf{x}(\Omega_n^k))=\sum_{i=1}^m\alpha_i p_i(\xi|\mu_i,\Sigma_i)=\sum_{i=1}^m\frac{\alpha_i}{\sqrt{(2\pi)^{d_x}|\det\Sigma_i|}}\times\exp\left[\frac{-1}{2}(\xi-\mu_i)^T\Sigma_i^{-1}(\xi-\mu_i)\right],\quad(1)$$

where ξ is a random variable in R^{d_x}, $\Theta=(\alpha_1,\ldots,\alpha_m,\mu_1,\ldots,\mu_m,\Sigma_1,\ldots,\Sigma_m)$ and $\Sigma_{i=1}^m\alpha_i=1$. Each probability p_i is a Gaussian distribution with mean vector μ_i and covariance matrix Σ_i to represent a cluster. We apply the electromagnetic expectation-maximization algorithm [27] to estimate the parameter Σ and assign each datum in $\mathbf{x}(\Omega_n^k)$ to one of the m clusters based on the maximum posterior probability. The optimal value m^* of m is determined by the information criterion of MDL [28–30]:

$$m^*=\arg\min_m\left\{-\ln\left\{\prod_{n=1}^k\sum_{i=1}^m\alpha_i p(x_n|\Theta)\right\}+\lambda J\ln(k)\right\},\quad(2)$$

Here, the first term on the right-hand side of Eq. (2) is the maximum log-likelihood of Eq. (1) with parameters Θ, all random variables x_i are identical and independent distributions, $J=(d^2+3d+2)m/2-1$ (i.e., $d\times m$ $[(d+1)dm/2,\ m-1]$ parameters of μ_i $[\Sigma_i,\ \alpha_i]$) is the number of free parameters in the model, and λ $(=1/2)$ is a scalar factor. Therefore, the collection Ω_n^k can be partitioned into m pairwise disjoint collections $\Omega_n^{k_i}=\{\omega_{n,j}^{k_i}|j=1,\ldots,N_i\}$, $i=1,\ldots,m$, where N_i is the number of points in $\mathbf{x}(\Omega_n^{k_i})$ and all points in $\mathbf{x}(\Omega_n^{k_i})$ belong to the same cluster. The conditional and clustered mean Euclidean distance is defined by

$$V_n^{(m,k)}(\mathbf{X}|\mathbf{Y})=\max_{i=2,\ldots,m}\left\{\frac{1}{k_1}\sum_{j=1}^{k_1}\|\mathbf{x}_{\omega_n}-\mathbf{x}_{\omega_{n,j}^{k_1}}\|^2,\frac{2}{N_i(N_i-1)}\times\sum_{(j_1,j_2)\in\Omega_n^{k_i}}\|\mathbf{x}_{\omega_{n,j_1}^{k_i}}-\mathbf{x}_{\omega_{n,j_2}^{k_i}}\|^2\right\},$$

where $j_1<j_2$ and $\|\cdot\|$ is a Euclidean distance. The local and

global interdependences $S_n^{(m,k)}(\mathbf{X}|\mathbf{Y})$ and $S^{(m,k)}(\mathbf{X}|\mathbf{Y})$ are defined as

$$S_n^{(m,k)}(\mathbf{X}|\mathbf{Y}) = \min\left\{\frac{V_n^{(k)}(\mathbf{X})}{V_n^{(m,k)}(\mathbf{X}|\mathbf{Y})}, 1\right\} \tag{3}$$

and

$$S^{(m,k)}(\mathbf{X}|\mathbf{Y}) = \frac{1}{N}\sum_{n=1}^{N} S_n^{(m,k)}(\mathbf{X}|\mathbf{Y}), \tag{4}$$

respectively. The quantity $S_n^{(m,k)}(\mathbf{X}|\mathbf{Y})$ $[S^{(m,k)}(\mathbf{X}|\mathbf{Y})]$ means the local [global] variation rate of the mean distance influenced by $\mathbf{Y}$ and is called the *locally [globally] adaptive similarity-based index* (ASI). Notably, the proposed method (i.e., ASI) is the same as the traditional method (i.e., SI) proposed by Arnhold *et al.* [21] as $m=1$.

To avoid spurious detection of synchronization due to short data, noise, bandpass filtering, and signal complexity [22,31], we developed a two-level process of computing the ASI in order to get a more significant representative. First, we consider the univariate significant level of the globally ASI between $\mathbf{X}$ and $\mathbf{Y}$ as $S_{\text{uni}}^{(m,k)}(\mathbf{X}|\mathbf{Y}) := \max\{S^{(m,k)}(\mathbf{X}|\mathbf{Y}) - \tilde{S}^{(m,k)}(\mathbf{X}|\mathbf{Y}), 0\}$, where $\tilde{S}^{(m,k)}(\mathbf{X}|\mathbf{Y})$ is the 95th percentile of the distribution for 19 univariate surrogates of $\mathbf{Y}$ [22], generated by the iterative-amplitude-adjusted Fourier transform (IAAFT) algorithm [32]. Second, the bivariate significant level of the globally ASI is defined by

$$S_{\text{bi}}^{(m,k)}(\mathbf{X}|\mathbf{Y}) := \begin{cases} \max\{S^{(m,k)}(\mathbf{X}|\mathbf{Y}) - \hat{S}^{(m,k)}(\mathbf{X}|\mathbf{Y}), 0\}, & \text{if } S_{\text{uni}}^{(m,k)}(\mathbf{X}|\mathbf{Y}) > 0, \\ 0, & \text{if } S_{\text{uni}}^{(m,k)}(\mathbf{X}|\mathbf{Y}) < 0, \end{cases} \tag{5}$$

where $\hat{S}^{(m,k)}(\mathbf{X}|\mathbf{Y})$ is the 95th percentile of the distribution for 19 bivariate surrogates [22], generated by the IAAFT algorithm. The whole process of the adaptive similarity-based approach is presented in the Appendix.

III. EXPERIMENTS

In order to demonstrate the capability of Eq. (5), we conducted one simulation and one real experiment to show that the proposed method can detect not only GS, but also $1:m$ or $n:1$ PS effectively.

A. Simulation

1. Model description

Consider a unidirectionally coupled chaotic system, proposed by Le Van Quyen *et al.* [20]:

$$\begin{aligned} \dot{x}_1 &= -\alpha(x_2 + x_3), \\ \dot{x}_2 &= \alpha(x_1 + 0.2x_2), \\ \dot{x}_3 &= \alpha[0.2 + x_3(x_1 - 5.7)], \\ \dot{y}_1 &= -\rho(y_1 - y_2), \\ \dot{y}_2 &= ry_1 - y_2 - y_1y_3 + cx_2^2, \\ \dot{y}_3 &= y_1y_2 - by_3, \end{aligned} \tag{6}$$

where $\rho=10$, $r=28$, and $b=8/3$. The term cx_2^2 can be thought of as a perturbation item. When $c=0$, this coupled system can be viewed as two independent systems, where the state variables (x_1,x_2,x_3) and (y_1,y_2,y_3) represent the celebrated Rössler and Lorenz systems, respectively. The parameter α $(=10)$ is used to adjust the time scale of the Rössler system. In the study, the 200-s data were simulated by using fourth- and fifth-order Runge-Kutta algorithms with $\Delta t=0.002$ for the system (6) with $c=10$. Note that $N=10^5$ $[200(\text{s})/\Delta t]$ in Eq. (4). In order to eliminate transients, the first 10^6 iterations were discarded. The globally ASI in Eq. (5) was applied to quantify the interdependence between two time series x_n $[=x_1(t_n)]$ and y_n $[=y_1(t_n)]$ in the simulation data, where t_n denotes the nth sampling time and $n \in \mathbb{N}$. We suitably chose the 200 nearest neighbors $\mathbf{x}(\Gamma_n^{200})$ $[\mathbf{y}(\Omega_n^{200})]$ for every reconstructed vector $\mathbf{x}_n$ $[\mathbf{y}_n]$ of x_n $[y_n]$ with the delay time $\tau_x=70$ $[\tau_y=38]$ and the embedding dimension $d_x=3$ $[d_y=3]$ as described in Fig. 1. Herein, we only consider the variation rate of the mean distance of $\mathbf{X}$ influenced by $\mathbf{Y}$ because the same procedure can be utilized to discuss the opposite direction.

2. Results

Based on the driver indices in Ω_n^{200} for some n in Fig. 1(a), the mutual neighbors $\mathbf{x}(\Omega_n^{200})$ in Fig. 1(b) can be divided into two clusters. To elucidate the cause of clusters, we analyzed the temporal structure of the driver indices in Ω_n^{200} by the time difference (TD). Herein, the TD between successive indices ω_i and ω_{i+1} in Ω_n^{200} is defined by $\Delta\omega_i=(\omega_{i+1}-\omega_i)\Delta t$. We drop the TD equal to Δt because it indicates that two points are very close in the temporal domain. By estimating the differences among the TDs of the driver indices in Ω_n^{200}, we found that these TDs locate nearby a lattice as in Fig. 2, where the vertical distance between the successive grid lines is about 0.2927. Similarly, the TDs based on the response indices in Γ_n^{200} are displayed in Fig. 2. The TDs for the collections Ω_n^{200} (Γ_n^{200}) are obviously a multiple of 0.2927 (0.5855). Consequently, it is reasonable that, from the tem-

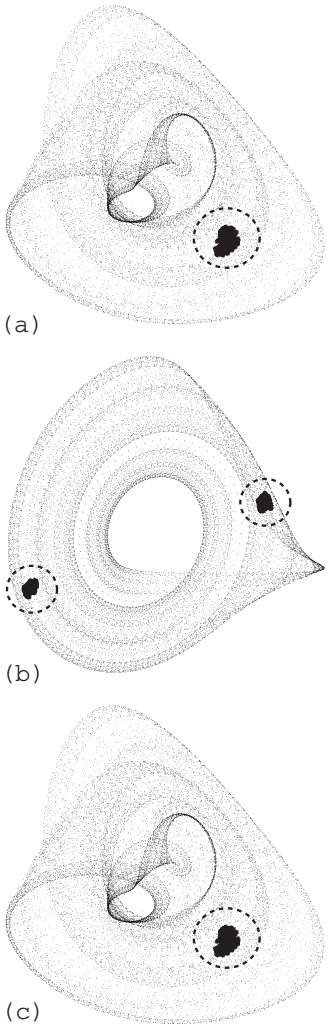

FIG. 1. (a) The reconstructed trajectory $\mathbf{Y}$ of a time series $y_1(t_n)$ with $\tau_{y_1}=38$ and $d_{y_1}=3$ is projected on a two-dimensional phase space. (b), (c) The reconstructed trajectory $\mathbf{X}$ of a time series $x_1(t_n)$ with $\tau_{x_1}=70$ and $d_{x_1}=3$ is projected on a two-dimensional phase space. The 200 actual neighbors $\mathbf{y}(\Omega_n^{200})$ $[\mathbf{x}(\Gamma_n^{200})]$ in (a) [(c)] are shown. The two-group black points in (b) represent the mutual neighbors $\mathbf{x}(\Omega_n^{200})$. Herein, $c=10$.

poral view, mutual neighbors $\mathbf{x}(\Omega_n^{200})$ are divided into two groups from the distributions of TDs for Ω_n^{200} and Γ_n^{200} in Fig. 2.

We analyzed the interdependence between $x_1(t)$ and $y_1(t)$ of the coupled system (6) with different values of the parameter $c \in [0,10]$ and show the results of the globally ASI and SI in Fig. 3(a). In Fig. 3(a), ASIs are all larger than SIs as $c>2.5$. It means that there exist some separable mutual neighbors. More specifically, we gave an example of the Rössler-Lorenz system with $c=10$ in Fig. 3(b), which showed the successive five time slots of mutual neighbors $\mathbf{x}(\Omega_\bullet^{200})$ in the reconstructed phase space. In these five figures, it is obvious that the black points were split from one group [i.e., *A* in Fig. 3(b1)] into two groups [i.e., *A* and *B* in Fig. 3(b2)], and later merged into one group [i.e., *A* in Fig. 3(b5)] again. After mutual neighbors $\mathbf{x}(\Omega_\bullet^{200})$ were modeled by the GMM with different numbers of groups, the optimal

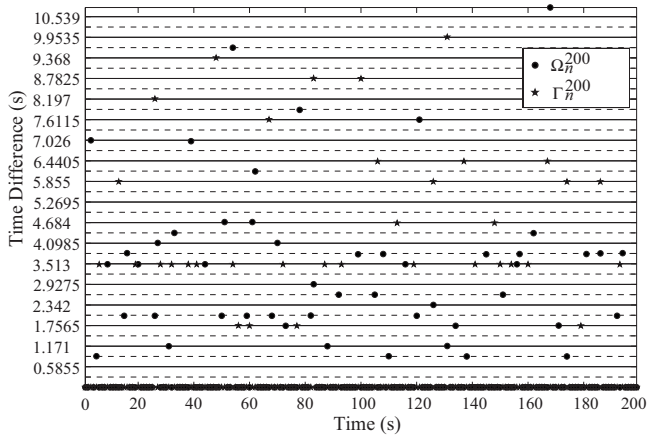

FIG. 2. Illustration of the TDs for the driver indices Ω_n^{200} and response indices Γ_n^{200} of the unidirectionally coupled system (6). Two kinds of horizontal lines, solid and dashed lines, are presented. The star (circle) points represent the TDs between the successive time points in KNN for the reconstructed trajectories X $[Y]$ in Fig. 1(c) [Fig. 1(a)], respectively. The star points only locate nearby the solid line. The circle points locate nearby these two kinds of lines. The minimum of TDs between the solid line and dashed one is 0.29275. Points nearby zero will be dropped due to the closeness of these points in their reconstructed phase spaces.

number of clusters determined by the MDL criterion was the same as the number of clusters in this simulated system. Consequently, for more complex synchronization, our method detected more features than the traditional one [21].

B. Self-paced finger movement

The aim of the real experiment is to detect the GS with $1:m$ PS between physiological signals by Eq. (5). The experiment design as follows is similar to that described in Tass *et al.* [7]. The contralateral primary sensorimotor cortex generally plays a role in the major corticospinal outflow during volunteer movements. Considering the human brain as a dynamical system with frequent changes of its functional mode, the task of self-paced finger movement can be proper to investigate the cortico-muscular representations within varied experimental designs.

1. Subjects and task

Four healthy, right-handed and well-trained subjects (whose ages ranged from 24 to 32 years old) were recruited for this experiment. All of them denied any neurological deficits and appeared naive with regard to the purpose of the experiment. They sat comfortably in a magnetically shielded room with open eyes. All participants were requested to perform repeated self-paced movement of the right index finger (35°–40° extension angles) at a time interval of 100 s with two tappings per 1 s in synchrony with a regular auditory pacing signal administered at 2 Hz (external pacing). Magnetic responses were measured by a 306-channel whole-head neuromangetrometer (Vector-view; Neuromag Ltd., Helsinki, Finland). We recorded the activity of the first dorsal in-

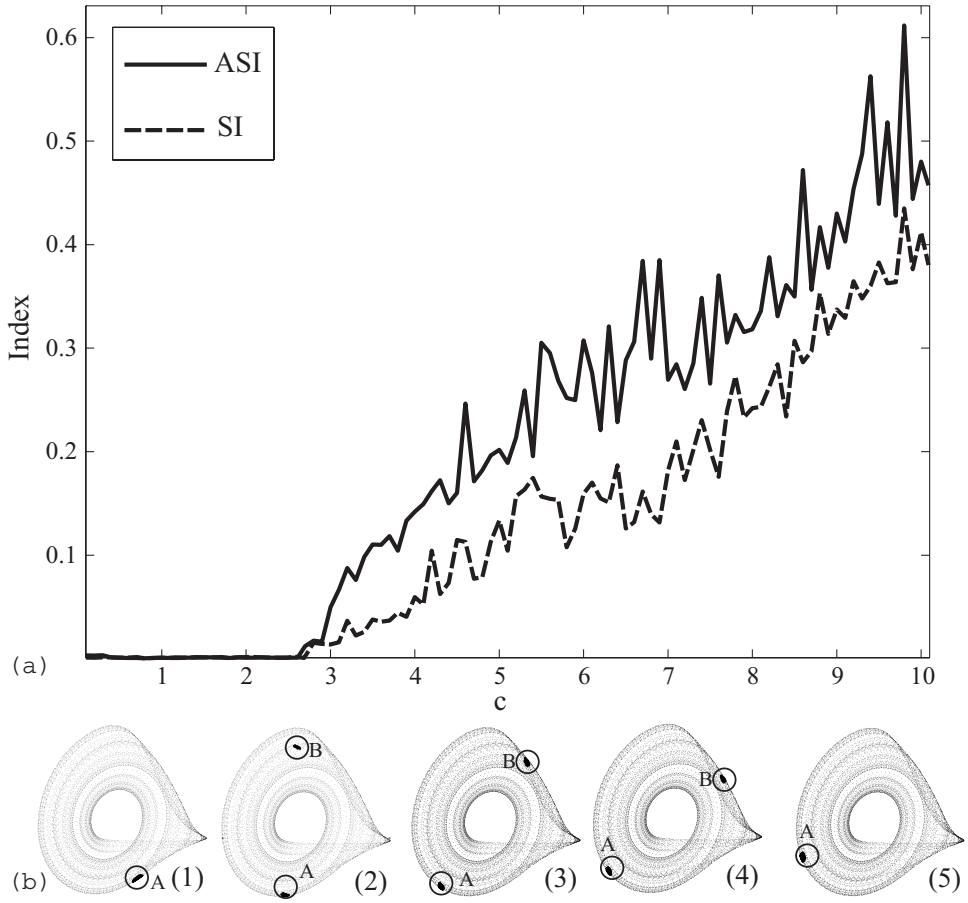

FIG. 3. (a) Description of the interdependence between time series $x_1(t)$ and $y_1(t)$ of the coupled system (6) by the measurement (5) (conventional SI) whose result is shown by the solid (dashed) line for $c \in [0,10]$. (b) Let $c=10$. We showed the diagram of the dynamics of the mutual neighbors $\mathbf{x}(\Omega_\bullet^{200})$ at five different sample times in the reconstructed Rössler system. Herein, the symbol • means a different point n (i.e., $\mathbf{x}_n$). The time of the from left to right in order is, respectively, from the early stage to the late one. The mutual neighbors $\mathbf{x}(\Omega_n^{200})$ in the circle A were split into two pieces A and B, later merged into one piece A.

terossei muscle of the right hand using a surface electromyogram (sEMG). The 30-s MEG and sEMG signals were simultaneously recorded with a bandpass filter of 0.03–330 Hz, digitized with 1 kHz, and stored digitally for off-line analysis. To avoid contamination related to movement vibrations during the MEG recordings, the subjects were asked to put their left forearms on a pillow at ease. To avoid the artifacts caused by eye movements, they also were requested to keep their eyes open and concentrate their focus on the fixed point in front of them. Here, we only describe the results of one subject due to the resemblance of the results for the remaining three subjects.

2. Results

The interdependence between the sEMG and one-task-related MEG (trMEG) signals was computed by Eq. (5), which only discussed the variation rate of the mean distance for the sEMG signal influenced by the trMEG signal. The power spectral analysis for the sEMG signal revealed a peak at 2 Hz. Hence, the sEMG signal was filtered with a narrow-band frequency corresponding to the principal sEMG frequency component of 2 Hz. The MEG signals recorded from gradiometer 1 at the 13th detector unit were chosen due to its neighboring the task-related cortical regions. To show GS with 1:2 PS, the trMEG signals were filtered with a bandpass extracting the 4-Hz band. The reconstructed trajectory of the filtered sEMG (trMEG) signal was constructed both with the time delay $\tau_{\mathrm{sEMG}}=120$ ($\tau_{\mathrm{trMEG}}=60$) ms and with the embedding dimension $d_{\mathrm{sEMG}}=10$ ($d_{\mathrm{trMEG}}=10$). The 200 nearest neighbors were chosen for these two reconstructed trajectories. Applying Eq. (5) to the reconstructed trajectories of the two filtered signals, we get the locally ASI in Fig. 4(a). The 1:2 phase difference between trMEG and sEMG signals was computed and the results are shown in Fig. 4(b). Herein, the phase difference is defined by $2\phi_{\mathrm{sEMG}}-\phi_{\mathrm{trMEG}}$ where ϕ_{sEMG} (ϕ_{trMEG}), the phase of the sEMG (trMEG), is extracted by Hilbert transformation. Comparing Figs. 4(a) and 4(c) with Fig. 4(b), the locally ASI appeared obviously more sensitive in detecting 1:2 PS than the conventional SI.

We elucidated the positions of actual and mutual neighbors at some time point in different ways. The 200 actual neighbors [mutual neighbors] are plotted in the two-dimensional projection of the reconstructed trajectory for the filtered sEMG signals in Fig. 5(a) [Fig. 5(b)] and are also represented in the corresponding time domain in Fig. 5(c) [Fig. 5(d)]. The 200 actual neighbors for the filtered trMEG

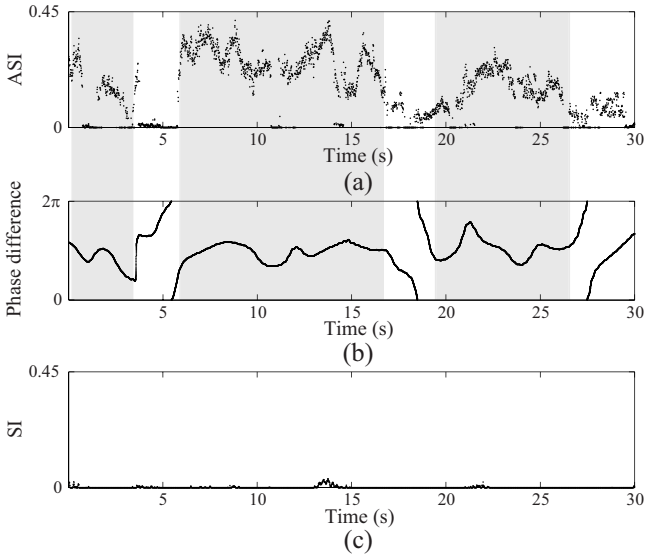

FIG. 4. (a) The locally ASI between the sEMG and trMEG is plotted during the 30-s period. All values in different times had subtracted $\hat{S}^{m,k}$(sEMG|trMEG). (b) We show the 1:2 phase difference between the sEMG and trMEG signals. (c) The conventional SI between sEMG and trMEG signals was computed without the GMM with MDL criterion.

are additionally shown in Fig. 5(e). To describe the relative positions between the actual and mutual neighbors, seven dashed lines are used to mark the positions between black points in Figs. 5(d) and 5(e). From visual inspection of Fig.

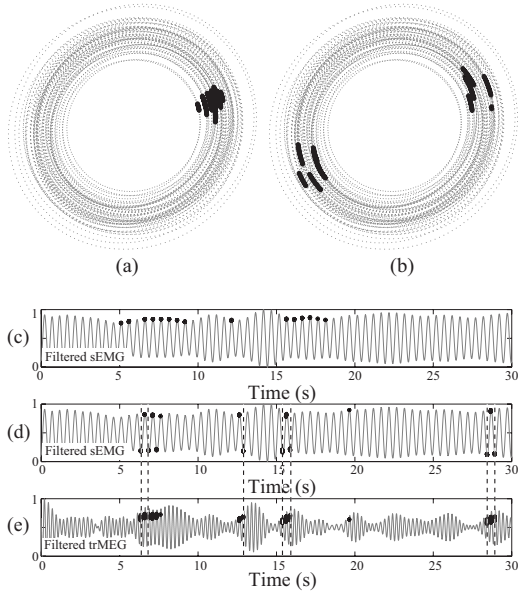

FIG. 5. The 200 actual [mutual] neighbors in (a) [(b)] are plotted in the two-dimensional projected and reconstructed trajectory of the filtered sEMG signal. For (c) and (d) [(e)], the sEMG signal [the trMEG signal from gradiometer 1 of the 13th detector unit] is filtered with a bandpass extracting the 2-Hz [4-Hz] narrow band. The actual (mutual) neighbors in (a) [(b)] represent the black points in (c) [(d)]. The black points in (e) represent the actual neighbors of the trMEG signal.

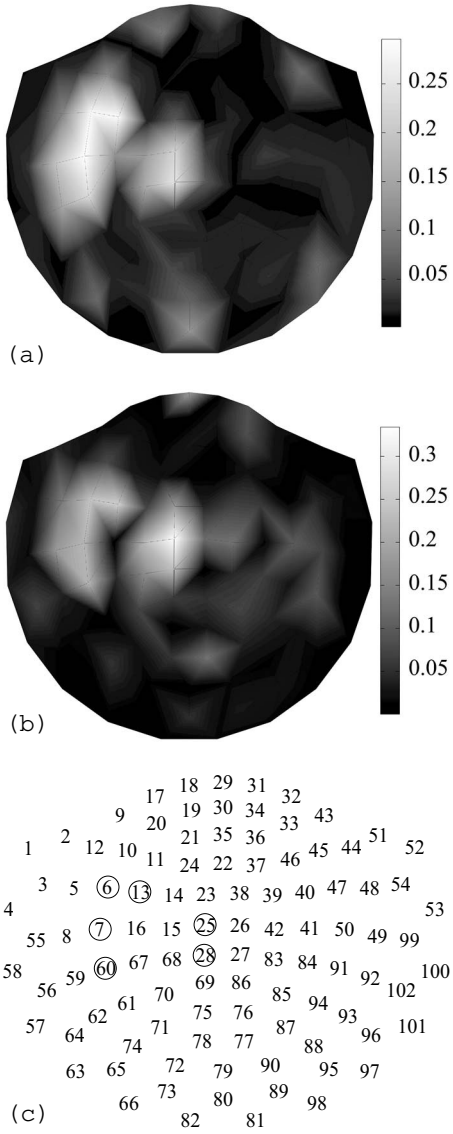

FIG. 6. The sEMG signal used as a response (or reference) system, the 102 globally ASIs between the filtered sEMG and MEG signals are shown in the topography as (a) and (b). Here, the sEMG (trMEG) signal is filtered with a bandpass extracting the 2-Hz band (the 4 or 6 Hz). (a) and (b) show the 1:2 and 1:3 PS between the trMEG and sEMG signals, respectively. In (c), the number of detector units corresponds to its position. We found that hot areas are nearby the motor area.

5(d) [Fig. 5(e), the phase difference of the successive black points is almost $\pi/2$ [π]. It is reasonable to have the two groups in Fig. 5(b) when we switch to the reconstructed phase space.

For other different MEG signals, the same strategy was applied to analyze the interdependence between the sEMG and individual MEG signals. It follows from the resulting brain topography in Fig. 6(a) that the signals located nearby sensorimotor cortex or premotor areas are highly synchronous to the sEMG signal. Even though the MEG signals were filtered with a bandpass extracting the 6-Hz band, Fig. 6(b) illustrates that GS with 1:3 PS exists between the task-related areas and the first dorsal interossei muscles of the

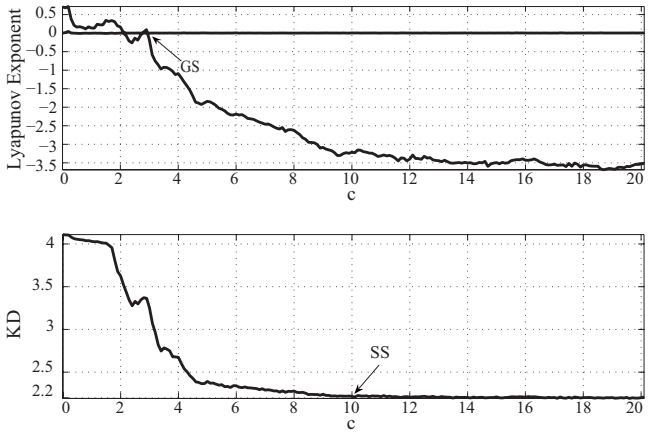

FIG. 7. Illustration of the bifurcation of Lyapunov exponent and KD for the coupled system (6).

right hand. In Fig. 6(c), the sensor numbers relative to hot areas are circled. These sensors are closest to the motor cortex in this sensor array. The results show that Eq. (5) was able to detect GS with $1:m$ PS between physiological signals for the task.

IV. DISCUSSION

The proposed method relies on the existence of GS as follows:

$$\mathbf{y}(n) = \mathbf{F}(\mathbf{x}(n)), \tag{7}$$

where $\mathbf{F}$ is a continuous function [17]. Here, we discuss a two-to-one continuous function $\mathbf{F}$ especially. If actual neighbors of $\mathbf{y}(n)$ have time indices n_{KNN}, the mutual neighbors $\mathbf{x}(n_{\mathrm{KNN}})$ can be represented by the union of two sets $\mathbf{x}(n'_{\mathrm{KNN}})$ and $\mathbf{x}(n''_{\mathrm{KNN}})$, where $n_{\mathrm{KNN}}=n'_{\mathrm{KNN}}\cup n''_{\mathrm{KNN}}$. The separable mutual neighbors can be viewed as two clusters. In this case, the closeness and connectivity of a continuous function is unsuitable to explain the separable neighbors. To detect the synchronization, influenced by $\mathbf{y}$, the clustering characteristic is superior to the closeness and connectivity of a continuous function in [17]. Even though a continuous function is one to one, the inseparable mutual neighbors are viewed as one cluster. Consequently, the clustering feature can describe more about synchronization than the feature of closeness and connectivity.

The occurrence of GS in a unidirectional coupled system can be detected by the negativeness of the maximum conditional Lyapunov exponent (CLE) [33]. This can be applied for the unidirectional coupled deterministic system (6) and infeasible for experimental data from self-paced finger movement. For the coupled system (6), the onset $c=2.92$ of GS is confirmed in Fig. 7. Additionally, the occurrence of strong synchronization (SS) (i.e., the existence of a smooth map) based on the criterion from Pyragas [34] is at $c\geq 10$, where the Kaplan-Yorke dimension (KD) [35] is almost constant in Fig. 7. At $2.92<c<10$, this functional relation between the driver and response system, therefore, is weak synchronization (WS) (i.e., the existence of an unsmooth map)

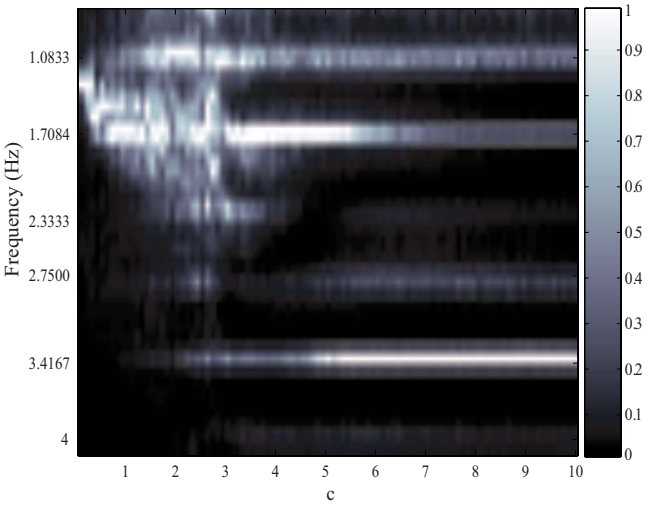

FIG. 8. (Color online) Illustration of the frequency of the time series $y_1(t_i)$ for different parameters c, a perturbation parameter in Eq. (6). The time scale parameter α is 10. Normalized frequency power spectrum utilizing fast Fourier transform and Hamming window was applied to time series $y_1(t_i)$ simulated for different parameters c.

and maybe has a fractal structure. The computation, therefore, provides the existence of GS of the coupled system (6) including SS and WS. This is discussed on their original manifolds. For the reconstructed state space, by Takens' embedding theorem [15], there exists diffeomorphism between an original manifold and its reconstructed one based on the time-delayed reconstruction if the dynamical system and the observed quantity are generic. Let $\mathbf{X_d}$ ($\mathbf{X_r}$) be a diffeomorphism from an original manifold to the reconstructed one for the driver (response) system. If a relation between two reconstructed manifolds for the driver and response system can be modeled by a function $\mathbf{F}$, then a relation $\bar{\mathbf{F}}$ between the original manifolds for the two subsystems can be written by the function $\bar{\mathbf{F}}=\mathbf{X_r}^{-1}\circ\mathbf{F}\circ\mathbf{X_d}$. Hence, the functional relationship between the original manifolds of two coupled subsystems can be equivalent to one between their reconstructed manifolds. Furthermore, the onset of GS on the original manifolds can be consistent with the positiveness of the ASI and SI on the reconstructed state space as $c>2.92$ in Fig. 3(a). Therefore, we indirectly show the reliability of detecting GS including SS and WS by the ASI and SI.

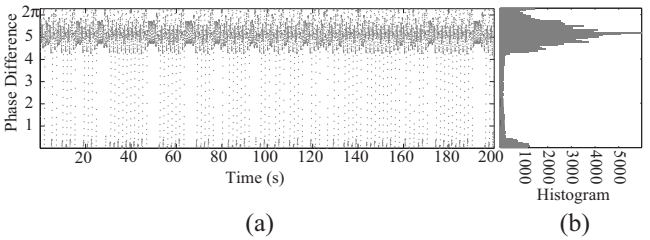

FIG. 9. (a) Illustration of the 2:1 phase difference $2\phi_{x_1}(t)-\phi_{y_1}(t)$ between two time series $x_1(t)$ and $y_1(t)$ of the coupled system (6). (b) Histogram of the 2:1 phase difference is computed from the result in (a).

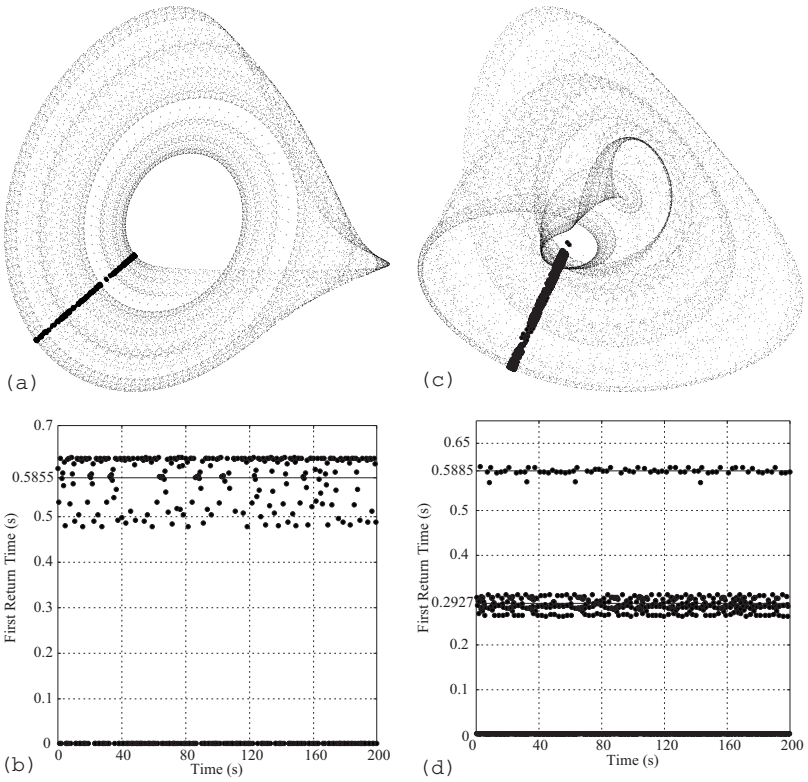

FIG. 10. For (a) [(c)], a reconstructed trajectory **X** [**Y**] of a time series $x_1(t)$ $[y_1(t)]$ for the Rössler-Lorenz system (6) is plotted with the same parameters as setting in Fig. 1. We choose points in a Poincaré sections of (a) [(c)] for computation of the first return time plotted in (b) [(d)]. Here, the two means 0.2927 and 0.5855 are highlighted. It is obvious that there is a multiple relation between these two average return times. Note that $c=10$.

We should make it clear about the similarity of two segmented time series in a time series when two points are close in its reconstructed state space. Let a point $\mathbf{x}_n$ in the reconstructed state space give as the previous definition and be written as $(x_n,\ldots,x_{n+(d_x-1)\tau})$. Under the ideal situation, the segmented time series in between the n and $n+(d_x-1)\tau$ sample times can be completely denoted by the d_x samples. Let $\tilde{\mathbf{x}}\in B_\delta(\mathbf{x}_n)$, where $\tilde{\mathbf{x}}=(\tilde{x}_1,\ldots,\tilde{x}_{d_x})$ and $B_\delta(\mathbf{x}_n)=\{\mathbf{x}\in\mathbb{R}^{d_x}|\|\mathbf{x}-\mathbf{x}_n\|^2=\delta\}$. When $\delta=0$, we assume that the two segmented time series in a time series have the same wave form for any two ponits in$B_0\mathbf{x}_n$. When $0<\delta\ll 0$, we assume that the two segmented time series in the time series are very similar for any two points in $B_\delta(\mathbf{x}_n)$. Hence, when the mutual neighbors in the response system are very close, we infer that their shapes are very similar to each other. On the contrary, the similar shapes in a time series represent the fact that the points in the reconstructed phase space will be close to each other under a suitable parameter, delay time, and embedding dimension. The two close points in the reconstructed phase space are, therefore, equivalent to the similar shapes in the time domain.

For the coupled system (6), a frequency-locked phenomenon will be described. The time series $x_1(t_i)$ has a natural frequency of about 1.7087 in the coupled system (6). For the time series $y_1(t_i)$, there are obviously frequencies 1.7084 and 3.4167. In Fig. 8, at the parameter $2.92<c<5$, the principal frequency of the time series $y_1(t_i)$ is the same as the nature frequency of $x_1(t_i)$. As the parameter $c>5$, the principal frequency ($\doteq$3.4167) of the Lorenz system is twice than the one ($\doteq$1.7084) of the Rössler system. By the frequency analysis, the frequency of the response system is dominated by the one of the driver system. Hence, there are frequency-locked phenomena between two subsystems. Additionally, comparing Fig. 3(a) with Fig. 8, there exists a transition at the parameter 2.92. One in Fig. 3(a) is the negativeness of CLE; the other in Fig. 8 is the transition of the frequency. We further show the existence of 2:1 PS in the system (6) with the parameter $c=10$ by the conventional Hilbert-based PS. The phase ϕ_{x_1} (ϕ_{y_1}) of signals x_1 (y_1) is computed after the construction of its analytic signals [36]. Computing their 2:1 phase difference, $2\phi_{x_1}-\phi_{y_1}$, we find that the interaction between variables x_1 and y_1 of the system (6) can lead to a locking of their phases as Fig. 9(a). The distribution of the phase difference as Fig. 9(b) has a low uncertainty. Consequently, we conclude that there exists 2:1 PS in some epochs. This result is stronger than the one by the frequency analysis. However, our method can provide the self-similarity between any two time series segmented from a time series. That is, there is correlation inside the time series of the response system. As our result in Fig. 5, we show the self-similarity for EMG signals. The proposed method can, hence, provide more information about phase than the conventional SI. For researchers who only want to know the phase-locked correlation between two time series, the conventional Hilbert-based PS has a good performance. The Hilbert-based method completely ignores the information of amplitude but phase. In other words, we ignore whether two segmented time series can be totally independent or there exist some patterns between them. However, when GS and mixed-type PS coexist, these two methods, SI- and Hilbert-based PS, cannot show the phenomenon. The existence of GS implies the predictability of the location. For the coupled system (6), we can simultaneously predict the two positions in the modified Lorenz system by the Rössler system.

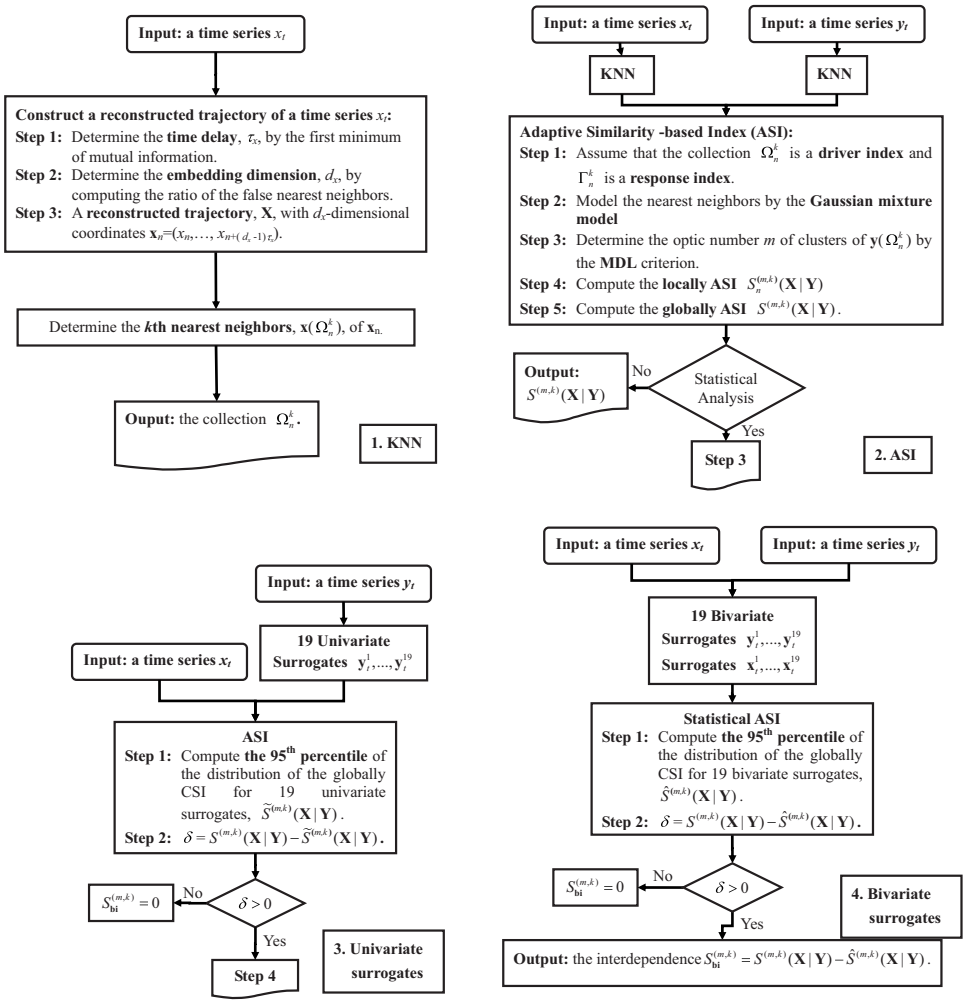

FIG. 11. Illustration of the flow chart of the adaptive similarity-based approach.

Since the clustering feature in the spatial domain is the key to the proposed method, we explain mechanisms for its occurrence in the coupled system (6) with $c=10$ by the averaged return time (ART). The result in Sec. III A 2 was only discussed in the nearest neighborhood; however, the ART is going to be discussed on a Poincaré section, the section transversally crossed by trajectories. The ART method is able to present the averaged time of the trajectories first returning to the Poincaré section. Let θ_x^n [θ_y^n] be the *first return time* of the mth crossing of the reconstructed Rössler trajectory for x_n (for the reconstructed Lorenz trajectory of y_n) through an appropriate Poincaré section in Fig. 10(a) [Fig. 10(b)]. Given the differences $\theta_x^{n+1}-\theta_x^n$ [$\theta_y^{n+1}-\theta_y^n$] as in Fig. 10(b) [Fig. 10(d)], we computed the ART $\langle\theta_x^{n+1}-\theta_x^n\rangle$ [$\langle\theta_y^{n+1}-\theta_y^n\rangle$] whose value is 0.5855 s [0.2927 s], where $\langle\cdot\rangle$ means averaging over m. Note that, for the reconstructed Lorenz trajectory of y_n, we only averaged the first return time in between 0.2 and 0.4, and there still exists the period 0.5855 of the averaged return time. The averaged return time for the reconstructed trajectory of y_n spends almost twice as much time as that of x_n returning to their own Poincaré section; i.e., $2\langle\theta_x^{n+1}-\theta_x^n\rangle \approx\langle\theta_y^{n+1}-\theta_y^n\rangle$. In other words, as points in the Rössler system return to their Poincaré section once, the corresponding points in the coupled system return to themselves once or twice. Besides, it follows from the frequency analysis that a time series x_n generated by the Rössler system in Eq. (6) has a natural frequency ω ($\approx$1.7084 Hz). By the formula $T=1/\omega$, where T is the period and ω is frequency, the period of the time series x_n is about 0.5855 s. The period of the corresponding time series y_n with respect to the frequency 3.4167 (1.7084) is about 0.2927 s (0.5855 s). The ratios of periods between two subsystems are almost multiple ($0.5855/0.2927\approx 2$, $0.5855/0.5855=1$). Hence, there are coherent results for both the ART in the spatial domain and frequency analysis in the temporal domain.

Depending on the numerical definition of Eq. (4), we give a mathematical presentation of the functional relationship for the coupled system (6) with $c=10$. The functional relationship is denoted by $\mathbf{y}(n)=\mathbf{F}(\mathbf{x}(n))$, where $\mathbf{x}(n)=(x_1(n),\ldots,x_1(n+(d_x-1)\tau_x))$ and $\mathbf{y}(n)=(y_1(n),\ldots,y_1(n+(d_y-1)\tau_y))$. Here $2\tau_y=\tau_x$ as in Sec. III A 1. Hence, $\mathbf{y}(n+kT_y)=\mathbf{F}(\mathbf{x}(n+kT_y))=\mathbf{F}(\mathbf{x}(n+\frac{k}{2}T_x))$ because $2T_y=T_x$. Herein, a period T is the reciprocal of its frequency ω. By the result of analyzing the conventional SI between $x_1(t_i)$ and $y_1(t_i)$, the variation rate of the mean distance exceeds statistically zero as $c=10$. In other words, the neighbors $\mathbf{y}(n+hT_y)$ of $\mathbf{y}(n+kT_y)$ can predict the neighbors $\mathbf{x}(n+\frac{h}{2}T_x)$ of $\mathbf{x}(n+\frac{k}{2}T_x)$, where $h\in\mathbb{R}$ and $\mathbf{y}(n+hT_y)$ are contained in the actual neighbors of $\mathbf{y}(n+kT_y)$. By the first return time analysis, a point in a Poincaré section almost takes T_x time back to the same

section. If a point $\mathbf{x}(n)$ takes $\frac{h}{2}T_x$ time, where h is odd, it travels just half the route of a period. If a point $\mathbf{x}(n)$ takes $\frac{h}{2}T_x$ time, where h is even, it travels just a route with a full period. So $\mathbf{x}\left(n+\frac{h_1}{2}T_x\right)$ and $\mathbf{x}\left(n+\frac{h_2}{2}T_x\right)$ with odd numbers h_1 and even numbers h_2 should be in different clusters. Hence, for this case, the ASI can describe more information about a phase-locked phenomenon than the conventional SI.

The clustering behavior became unpredictable because of different averaged return times. The Gaussian mixture models with the MDL criterion were therefore used to adaptively cluster points. The models have been proposed for quite some time as a basis for cluster analysis. In our proposed process, the distribution of the nearest neighbors was assumed as a mixture of Gaussian distributions, each representing a different cluster. To our knowledge, the model-based classification can match the clinical classification of a biomedical data set much more closely than the single-link or standard k means. Hence, the model-based classification was applied to distinguish different neighbors. In addition to the MDL criterion, there are three more criteria: the Akaike information criterion [37], the Bayesian information criterion [28], and cross-validation [38]. Since the maximized log-likelihood could be registered as a goodness-of-fit measure for all four methods, the optimal number of clusters can be decided accordingly.

The present work has great potential in many applications. The globally ASI can be ideally used to model the functional relation between systems as a many-to-one continuous function. When the globally ASI is larger than the conventional SI (i.e., ASI with only one cluster), it implies that a many-to-one continuous function exists and the coupled system possesses GS with PS. In the case of the one-to-one continuous function, only the GS would be detectable. Our method is also capable of detecting that the coupled system is GS with mixed types of PS (e.g., coexistence of GS and PS) in which the clustering behaviors are irregular.

V. CONCLUSIONS

The current study has established the ASI which effectively quantifies GS with $n:m$ PS between two subsystems with clustering behaviors within the response system, where at least one of n and m is 1. The salient features of this method included (i) trajectory reconstruction for transforming a temporal domain into a spatial domain, (ii) cluster analysis for dynamically detecting the clustering characteristic in the response space, and (iii) surrogate data for reducing the effect of noise, bandpass filtering, and its complexity. When applied to the unidirectionally coupled Rössler-Lorenz system, the globally ASI could detect the nonlinear interdependence more sensitively than the SI after implementation of cluster analysis with the Gaussian mixture model and MDL criterion. Furthermore, when applied to the data of the self-paced finger movement, the globally ASI could successfully detect GS with 1:2 and 1:3 PS between the physiological (i.e., sEMG to MEG) signals. Thus, the proposed adaptive method provides a promising tool to probe the synchronization characteristics in nonlinear dynamics and brain science.

ACKNOWLEDGMENTS

This study was funded by the Taipei Veterans General Hospital (Grants Nos. V95ER1-003 and V96C1-029) and the National Science Council (Grants Nos. NSC94-2811-B-075-002, NSC-95-2752-B-010-006-PAE, NSC96–2115–M-003–011–MY2, and NSC95–2752–B-010–007–PAE).

APPENDIX: THE FLOW CHART OF ANALYSIS

The flow chart of detecting GS with $1:m$ PS between two time series is illustrated in Fig. 11. In step 1, we describe both how to reconstruct a trajectory of a time series and how to decide the k nearest neighbors of points. In step 2, we describe the flow chart of computing the globally ASI without surrogates. In step 3 (step 4), we show the flow chart of computing the globally ASI with univariate (bivariate) surrogates.

[1] C. J. Stam, B. F. Jones, I. Manshanden, A. M. van Cappellen van Walsum, T. Montez, J. P. A. Verbunt, J. C. de Munck, B. W. van Dijk, H. W. Berendse, and P. Scheltens, Neuroimage **32**, 1335 (2006).
[2] D. Rudrauf, A. Douiri, C. Kovach, J. P. Lachaux, D. Cosmelli, M. Chavez, C. Adam, B. Renault, J. Martinerie, and M. Le Van Quyen, Neuroimage **31**, 209 (2006).
[3] C. Carmeli, M. G. Knyazeva, G. M. Innocenti, and O. De Feo, Neuroimage **25**, 339 (2005).
[4] A. Schnitzler and J. Gross, Nat. Rev. Neurosci. **6**, 285 (2005).
[5] O. David, D. Cosmelli, and K. J. Friston, Neuroimage **21**, 659 (2004).
[6] P. A. Tass, Biol. Cybern. **91**, 203 (2004).
[7] P. A. Tass, T. Fieseler, J. Dammers, K. Dolan, P. Morosan, M. Majtanik, F. Boers, A. Muren, K. Zilles, and G. R. Fink, Phys. Rev. Lett. **90**, 088101 (2003).
[8] M. G. Rosenblum, A. S. Pikovsky, J. Kurths, G. V. Osipov, I. Z. Kiss, and J. L. Hudson, Phys. Rev. Lett. **89**, 264102 (2002).
[9] F. Varela, J. P. Lachaux, E. Rodriguez, and J. Martinerie, Nat. Rev. Neurosci. **2**, 229 (2001).
[10] J. P. Lachaux, E. Rodriguez, M. Le Van Quyen, A. Lutz, J. Martinerie, and F. J. Varela, Int. J. Bifurcation Chaos Appl. Sci. Eng. **10**, 2429 (2000).
[11] J. P. Lachaux, E. Rodriguez, J. Martinerie, and F. J. Varela, Hum. Brain Mapp. **8**, 194 (1999).
[12] P. Tass, M. G. Rosenblum, J. Weule, J. Kurths, A. Pikovsky, J. Volkmann, A. Schnitzler, and H. J. Freund, Phys. Rev. Lett. **81**, 3291 (1998).
[13] M. Le Van Quyen, J. Foucher, J. Lachaux, E. Rodriguez, A. Lutz, J. Martinerie, and F. Varela, J. Neurosci. Methods **111**,

83 (2001).
[14] M. G. Rosenblum, A. S. Pikovsky, and J. Kurths, IEEE Trans. Circuits Syst., I: Fundam. Theory Appl. **44**, 874 (1997).
[15] F. Takens, *Dynamical Systems and Turbulence* (Springer-Verlag, Berlin, 1981).
[16] T. Sauer, J. Yorke, and M. Casdagli, J. Stat. Phys. **65**, 579 (1991).
[17] N. F. Rulkov, M. M. Sushchik, L. S. Tsimring, and H. D. I. Abarbanel, Phys. Rev. E **51**, 980 (1995).
[18] M. Le Van Quyen, C. Adam, M. Baulac, J. Martenierie, and F. Varela, Brain Res. **792**, 24 (1998).
[19] S. J. Schiff, P. So, T. Chang, R. E. Burke, and T. Sauer, Phys. Rev. E **54**, 6708 (1996).
[20] M. Le Van Quyen, C. A. Martinerie, and F. J. Varela, Physica D **127**, 250 (1999).
[21] J. Arnhold, P. Grassberger, K. Lehnertz, and C. E. Elger, Physica D **134**, 419 (1999).
[22] E. Pereda, R. Rial, A. Gamundi, and J. Gonzalez, Physica D **148**, 147 (2001).
[23] R. Quian Quiroga, J. Arnhold, and P. Grassberger, Phys. Rev. E **61**, 5142 (2000).
[24] M. Paluŝ and M. Vejmelka, Phys. Rev. E **75**, 056211 (2007).
[25] A. M. Fraser and H. L. Swinney, Phys. Rev. A **33**, 1134 (1986).
[26] L. Cao, Physica D **110**, 43 (1997).
[27] A. P. Dempster, N. M. Laird, and D. B. Rubin, J. R. Stat. Soc. Ser. B (Methodol.) **39**, 1 (1977).
[28] G. Schwarz, Ann. Stat. **6**, 461 (1978).
[29] P. Grünwald, J. Math. Psychol. **44**, 133 (2000).
[30] S. de Rooij and P. Grünwald, J. Math. Psychol. **50**, 180 (2006).
[31] J. Theiler, S. Eubank, A. Longtin, B. Galdrikian, and J. D. Farmer, Physica D **58**, 77 (1992).
[32] T. Schreiber and A. Schmitz, Physica D **142**, 346 (2000).
[33] L. Kocarev and U. Parlitz, Phys. Rev. Lett. **76**, 1816 (1996).
[34] K. Pyragas, Phys. Rev. E **54**, R4508 (1996).
[35] P. Frederickson, J. L. Kaplan, E. D. Yorke, and J. A. Yorke, J. Diff. Eqns. **49**, 185 (1983).
[36] D. Gabor, J. Inst. Electr. Eng., Part 1 **93**, 429 (1946).
[37] H. Akaike, in *Proceedings of the Second International Symposium on Information Theory, Tsahkadsor, 1971*, edited by B. N. Petrov and F. Csaki (Akadémiai Kiadó, Budapest, 1973), pp. 267–281.
[38] M. W. Browne, J. Math. Psychol. **44**, 108 (2000).